Proceedings of the Thirtieth (2020) International Ocean and Polar Engineering Conference **www.isope.org**
Shanghai, China, October 11-16, 2020

ISBN 978-1-880653-84-5; ISSN 1098-6189

A Parametric Method for Submerged Floating Tunnel Cross-section Design

P.X. Zou
Department of Hydraulic Engineering, Delft University of Technology, Delft, The Netherlands
CCCC FHDI Engineering Co., Ltd. Guangzhou, Guangdong, China
CCCC SFT Technical Joint Research Team Zhuhai, Guangdong, China

Jeremy D. Bricker
Department of Hydraulic Engineering, Delft University of Technology
Delft, The Netherlands

Wim Uijttewaal
Department of Hydraulic Engineering, Delft University of Technology
Delft, The Netherlands

ABSTRACT

A submerged floating tunnel's (SFT) cross-sectional geometry is one of the main factors influencing its hydrodynamic characteristics. Minimizing the drag and lift is important for reducing the displacement of the structure and load on the mooring system. In this study, a parametric cross-section design method based on the Bézier curve is used to define the geometry of the SFT cross-section. A sensitivity analysis of the Bézier curve parameters is conducted with Computational Fluid Dynamics (CFD), and compared with simpler common cross-sections. The results show the parametric design method noticeably reduces the mean drag and RMS lift coefficient, compared with simpler common sections.

KEY WORDS: Submerged floating tunnel; cross-section; Bézier curve; CFD.

INTRODUCTION

The submerged floating tunnel (SFT), as a novel deep sea or lake crossing, has distinct advantages of shortening the waterway crossing distance, reducing the cost of foundation retreatment, increasing the environmental adaptability, and has no impacts on navigation (Yan et al. 2016; Minoretti et al. 2019; Jin and Kim 2018). Increasingly, research on the SFT hydrodynamic analysis and coupled system interaction has been conducted in recent years (Jin et al. 2017; Jin and Kim 2019; Kang et al. 2019). As one of the main design factors concerning the SFT hydrodynamic performances, the SFT cross-sectional geometry should be taken as a priority to be optimized at the feasibility analysis stage of design. An SFT cross-section with good hydraulic properties can minimize the drag and lift of the structure, reduce the displacements of the main tube body, decrease the load on the mooring system and hence, save the material cost for the construction. A typical SFT system arrangement in the sea is shown in Fig.1.

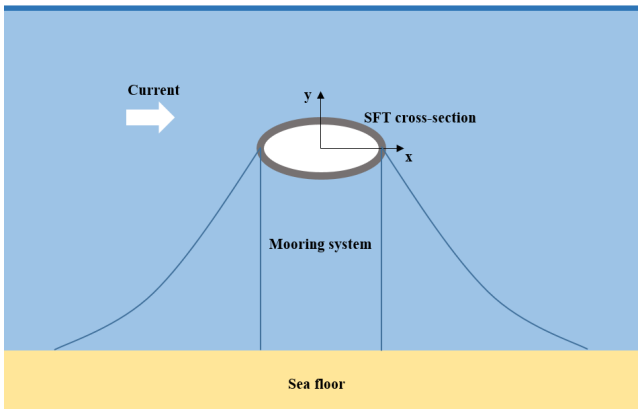

Fig.1 2D schematic configuration of an SFT system

Li et al. (2018) conducted an experiment in a water flume to compare the pressure distribution and wave forces of three kinds of SFT cross sections including circle, ellipse and polygon, and concluded that wave forces on the ellipse and polygon are smaller than on the circular shape. Luo et al.(2012) compared simulation results with five simple SFT forms and concluded that an SFT with a so called ear-shaped cross-section can withstand large ambient pressures, has good stability, and induces a smaller lift and drag force, resulting in the most reasonable cross-sectional shape. Li and Jiang (2016) compared the pressure distributions of elliptical and square SFT cross sections by combining

fluid mechanical calculation and structural analysis, concluding that the elliptical cross-section has smaller displacements and stresses than the rectangular section due to the streamlined shape. Gang et al. (2018) conducted explosion shock wave response analysis of rectangular, circular, and elliptical SFT cross sections by using the finite element software LS-DYNA, and concluded that the peak velocity of the elliptical shape is the smallest.

So far, based on SFT cross-section analysis achievements, the elliptical and ear-shaped SFT cross-section shapes have good hydrodynamic characteristics compared with other simpler cross-section geometries including circle, polygon, and square (Li and Jiang 2016; Luo et al. 2012, Gang et al. 2018). However, only simple SFT cross-sections have been focused on, and a detailed parametric method to define SFT cross-section still lacking. Additionally, comparing with the profile design in other fields such for airfoils and turbine blades, the potential flow theory and the Kutta condition (Crighton 1985) can't be used for the bluff SFT shape due to strong flow separation, and the uncertain ambient flow angle of attack on the SFT cross-section, making the flow field around, and analysis of, the SFT cross-section complicated.

In this study, a parametric Bézier curve method is applied to describe the SFT cross-section, a sensitivity analysis of the Bézier curve parameters and main hydraulic properties are obtained by the ANSYS Fluent version 19.1 CFD solver running parallel computations. Comparison of hydraulic performance is made with simpler SFT cross-section shapes including elliptical and ear-shaped cross sections.

PARAMETRIC CROSS-SECTION DESIGN

With the references of airfoil shape design as used in the previous research (Derksen and Rogalsky 2010; Nikolaev 2019; Jung et al. 2016), a parametric Bézier curve based on a Bézier-PARSEC (BP) method is employed to describe the SFT cross-section (Kharal and Saleem 2012), which combines the advantages of Bézier variables and PARSEC parameters. Bézier curves have a limited number of degrees of freedom determined by the control points. The PARSEC method makes it desirable to determine the parameters including the SFT cross-section dimensions such as the tunnel height and width.

Due to the indeterminacy of flow direction, a symmetrical shape of the SFT cross section should be considered at both the leading and trailing sides. Additionally, the pressure difference between the upper and lower surface can reflect the magnitude of lift, a symmetric shape of the upper and lower part can minimize the lift variation. Thus, the Bézier parameterization method can be expressed by only considering a quarter of the leading edge thickness curve, and the other parts are assumed symmetrical to the quarter curvature leading edge. Thus, the Bézier curve used in description of the SFT cross-section can be simplified compared with the traditional airfoil shape design. The parametric Bézier curve and control points are shown in Fig.2.

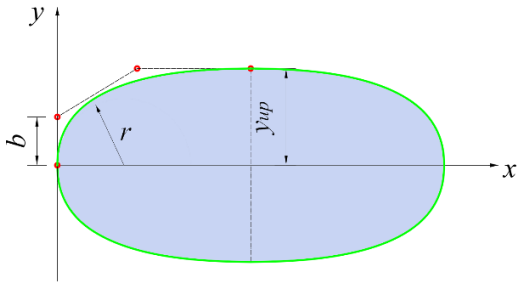

Fig.2 Third-degree Bézier curve. Note: red points are the control points

The third-degree parametric Bézier curves are used for the definition of the SFT cross-section, which is given by Eq.(1)

$$x(u) = x_0(1-u)^3 + 3x_1u(1-u)^2 + 3x_2u^2(1-u) + x_3u^3$$
$$y(u) = y_0(1-u)^3 + 3y_1u(1-u)^2 + 3y_2u^2(1-u) + y_3u^3 \quad (1)$$

Where u is a variable with the variation range of 0~1.

The four control points that determine the quarter curvature of the SFT cross-section are given by Eq.(2)

$$\begin{aligned} x_0 &= 0 & y_0 &= 0 \\ x_1 &= 0 & y_1 &= b \\ x_2 &= 3b^2/2r & y_2 &= y_t \\ x_3 &= x_t & y_3 &= y_t \end{aligned} \quad (2)$$

where r is the leading edge radius; b is subject to the following restriction

$$0 < b < \min\ (y_t, \sqrt{2rx_t/3})$$

Fig.3 shows a typical Two-Lane road tunnel cross section. Referring to the current standard criteria and feasibility study for the road tunnel and SFT cross section (Tveit 2000; Muhammad et al. 2017; American Association of State Highway Transportation Officials 2018; Ministry of Transport of the People's Republic of China 2010), the vertical clearance of SFT cross-section H=5m and width clearance of SFT cross-section W=10m with a fixed aspect ratio of 0.5 are applied for the sensitivity analysis in this study. As a symmetrical profile of the SFT cross-section, the remaining variables are main including y_{up} (y at upper side of the SFT cross-section), r and b. A sensitivity analysis of these Bézier curve parameters should be conducted to determine the appropriate cross-section parameter combinations.

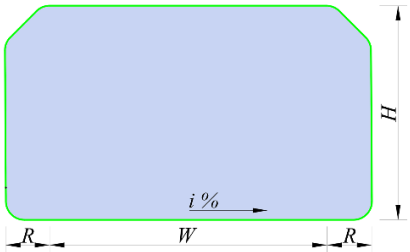

Fig.3 Typical two-lane tunnel cross section. Note: R is the curb or sidewalk; i is slope.

MODELING VALIDATION

The two-dimensional (2D) numerical simulation of the SFT cross-section with various Bézier curve parameters are designed in coupling with computer-aided design (CAD) tools and the ANSYS Design Modeler. The mesh of the computation domain is generated by ANSYS Mesh. The Grid Independent Limit (GIL) test is carried out to ensure the mesh convergence and validation of computational results. The triangular elements with the outer maximum element size 1m and the inner minimum element size 0.01m are chosen for all the analyzed cases. With the advantages of accurate simulation on dramatically changed geometry and flow separation with an additional term in ε equation, the RNG k-ε turbulence model with the standard wall-function is adopted. The Pressure-Implicit with Splitting of Operators (PISO) algorithm is applied for pressure-velocity coupling. The boundary condition at the sides and cylinder wall is adopted as "Non-slip" wall condition. The "velocity-inlet" boundary condition with a

uniform flow speed 0.1m/s is employed at the inlet. The zero reference pressure and zero-gradient condition for velocity is employed at the pressure-outlet boundary. The wall roughness of the SFT surface is assumed as 3mm. The boundaries are appropriate to set the inlet and lateral boundaries 5W away from the cylinder axis, and 15W away for the outlet boundary, relying on the sensitivity analysis. The maximum CFL number is restricted to 0.5 for the stability. The computational domain is shown in Fig.4.

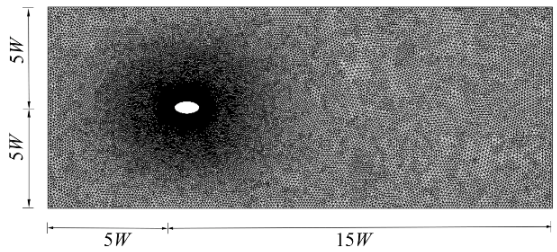

Fig.4 Schematic diagram of the computational domain

Considering the prototype scale of the SFT cross-section and current speed in deep sea, the Reynolds number has a magnitude of 10^6 or even higher, encompassing both supercritical ($4\sim5\times10^5$ and $2.5\sim4\times10^6$) and transcritical ($>2.5\sim4\times10^6$) flow régimes (James et al.1980). Because sufficient experimental data is available, herein $Re=1\times10^6$ is selected to verify the accuracy of the numerical simulation results. The main hydraulic properties including the mean drag and pressure coefficients along the cylinder are compared with the published experimental data by James et al. (1980). A cylinder with diameter D=10m having the same Reynolds number and relative surface roughness (the ratio of surface roughness to model diameter) as the experiment was applied in validation. The Reynolds number (Re) is defined as Eq.(3)

$$\mathrm{Re}=\frac{\rho U d}{\mu} \tag{3}$$

where U is the uniform cross-flow velocity at the inlet boundary, here U=0.1m/s; ρ is fluid density; μ is fluid dynamic viscosity; d is the characteristic length in terms of diameter for a cylinder, chord length for airfoil, and clearance width W for SFT cross-section analysis.
The distribution of the mean pressure coefficient C_p around the cylinder is compared with the experimental data measured in the counterclockwise direction in Fig.5 (a) and given by Eq.(4)

$$C_p=\frac{p-p_{ref}}{\frac{1}{2}\rho U^2} \tag{4}$$

where p is the pressure on the cylinder; p_{ref} is the reference pressure. Fig.5 (b) shows the drag coefficient validation results. In order to verify the drag coefficient distribution clearly in the drag crisis region, Re= 6×10^5, 2×10^6, 4×10^6, 6×10^6, 1×10^7 are also added for the numerical simulation validation. The numerical results exhibit a reasonable and satisfactory agreement with the experimental data.

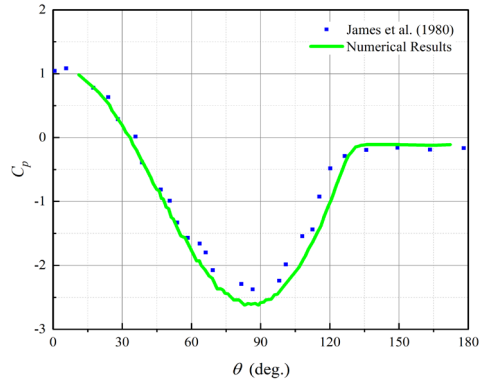

(a)

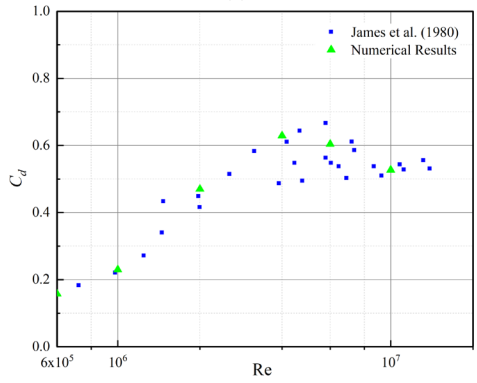

(b)

Fig.5 Numerical results validation. (a) C_p ; (b) C_d

RESULTS AND DISCUSSION

Sensitivity analysis of y

In order to optimize hydraulic performance of the SFT cross-section, the objectives of the SFT cross-section design should be to decrease the variation in the amplitude of lift and drag force ($F_{l,d}$) due to the uncertainty of current velocity and direction; hence the fluctuation amplitude of non-dimensional force coefficients should be applied as judging indexes. The drag and lift coefficients: C_d and C_l are given in Eq. (5).

$$C_{l,d}=\frac{F_{l,d}}{\frac{1}{2}\rho U^2 W} \tag{5}$$

Since the fluctuation amplitude of C_d is extremely small compared with the mean C_d, while the fluctuation of C_l is larger than the mean C_l, the mean drag coefficient $C_{d,m}$ is used, and the variability of C_l can be represented by its Root Mean Square (RMS) value, expressed as $C_{l,rms}$. To obtain reliable statistics, herein an unsteady simulation of 4000 non-dimensional time steps is conducted and the last 600 time steps are used for statistics.

Fig. 6 shows the trends of $C_{l,rms}$ and $C_{d,m}$ for the cases b=1 m, r=3 m and y_{up}=3.5 m, 3 m, 2.5 m, 2 m, 1.5 m. Since the total height of the SFT cross-section is fixed and equals 5 m, decreasing y_{up} means increasing y_{low}. Thus, the variables are symmetric around y_{up} =2.5 m. Note that $C_{l,rms}$ and $C_{d,m}$ are minimum when y_{up} =2.5 m, which is the half of the total SFT cross-section height, while $C_{l,rms}$ and $C_{d,m}$ increase dramatically with y_{up} when y_{up} >2.5 m. The above conclusions agree with experimental results for a thin flat plate in a water tunnel (Pelletier and Mueller 2000).

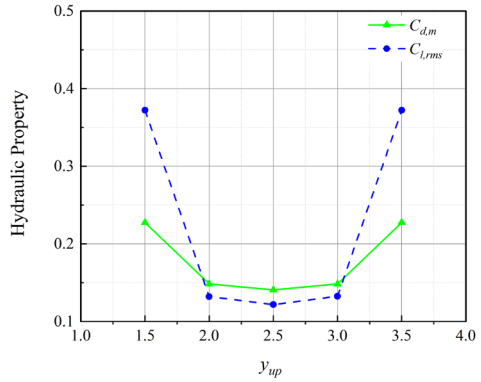

Fig.6 Hydraulic properties as a function of y

Sensitivity analysis of r

Fig.7 shows the trends of $C_{l,rms}$ and $C_{d,m}$ for the cases b=0.5 m, y_{up}=2.5 m, and r=0.1 m, 0.5 m, 1.0 m, 1.5 m, 2.5 m, 4.5 m. It can be seen that $C_{d,m}$ and $C_{l,rms}$ decrease remarkably and then increase slightly with increasing r, and obtains a minimum value around r =2.5 m. When r=0.1 m, a sharp leading edge and apex shape is generated due to the extremely small leading edge radius, resulting in a complete flow detachment from the apex and nadir points, and the larger suction pressure and a wider wake recirculation region at the rear surface, and hence increases the $C_{l,rms}$ and $C_{d,m}$.

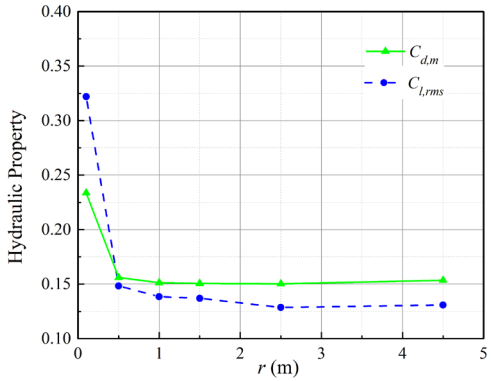

Fig.7 Hydraulic properties as a function of r

Sensitivity analysis of b

Fig.8 shows the trends of $C_{l,rms}$ and $C_{d,m}$ for the cases b=0.1 m, 0.5 m, 1.2 m, 1.8 m, 2.4 m, r=4.5 m, and y_{up} = 2.5 m. Both $C_{d,m}$ and $C_{l,rms}$ slightly and then sharply increase with increasing b. This is due to the SFT cross-section being bluffer as b increases, but no substantial geometry change when b<1.2 m. It can be concluded that a large b value should be avoided in the parametric SFT cross-section design with a fixed aspect ratio.

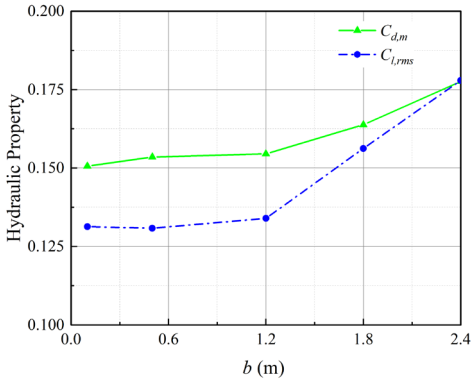

Fig.8 Hydraulic properties as a function of b

From the sensitivity analysis results of these Bézier curve parameters under a fixed aspect ratio, it should be noted that only changing one parameter doesn't always result in a continuously increasing or decreasing trend of $C_{d,m}$ and $C_{l,rms}$. It is the combined effect of these parameters, making the parametric SFT cross-section design complicated. Additionally, the SFT cross-section design should be balanced in the consideration of the arrangement, inclined angle, and stiffness of the mooring system, and the adjustment ability of SFT net buoyancy.

Comparison of different shapes

From all the parameter combinations mentioned above, the case with b= 1 m, r=3 m and y_{up}=2.5 m shows the minimum $C_{l,rms}$ and $C_{d,m}$. In order to show a streamlined shape and hydraulic property of the SFT cross-section defined by the parametric Bézier curve method, a comparison of the parametric Bézier curve method using the above parameter combination case is conducted under the same boundary conditions and tunnel height and width with the simpler SFT cross-section shapes. Fig.9 shows the results for $C_{l,rms}$ and $C_{d,m}$ with different SFT cross-section shapes based on the parametric Bézier curve method and simpler shapes including ellipse and ear shape with the same aspect ratio. It can be seen that the SFT cross-section determined by the paramedic design method has the minimum value of both $C_{l,rms}$ and $C_{d,m}$. $C_{d,m}$ using the parametric design method reduced by 3.5% and 29.6% compared with the ellipse shape and ear shape, respectively. $C_{l,rms}$ using the parametric design method is reduced by 13.1% and 42.6% compared with the ellipse shape and ear shape, respectively.

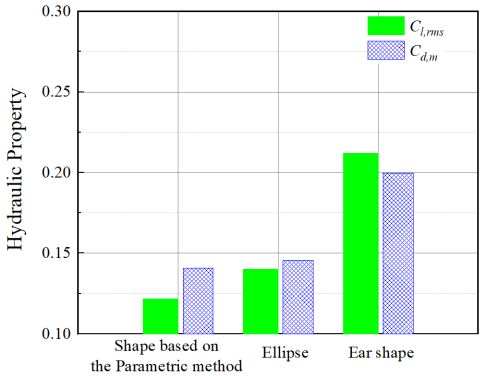

Fig.9 Comparison of hydraulic properties of different shapes

Fig.10 shows the instantaneous velocity contours of different shapes when lift curves reach their peak value. At the trailing edge, the flows along the upper and lower SFT cross-section surface with two separated shear layers coincide, approach, curve inwards and interact

with each other, forming the von Karman vortex street. From Fig.10, it is seen that the ear shape generates the largest wake region, vortex pattern, and the longitudinal and lateral consecutive vortex spacing, compared with the other shapes.

Fig.11 shows the mean pressure coefficient distributions along the SFT cross-section surface of different shapes. It shows that ear shape has two noticeable pressure valleys approximately located at x=2 m and x=8 m due to the blunter corners, and the ellipse shape has a valley near the apex point; while the parametric Bézier curve shape has a uniform pressure distribution along the SFT cross-section surface, reflecting the most streamlined shape compared with the two simpler shapes.

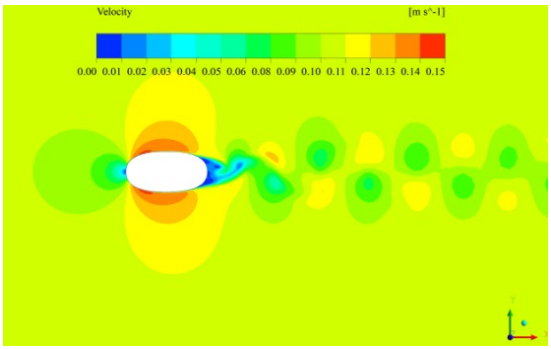

(a)

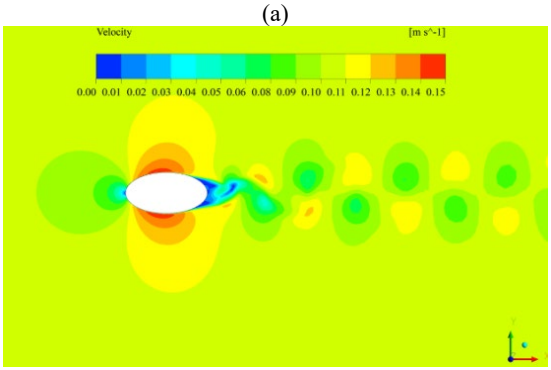

(b)

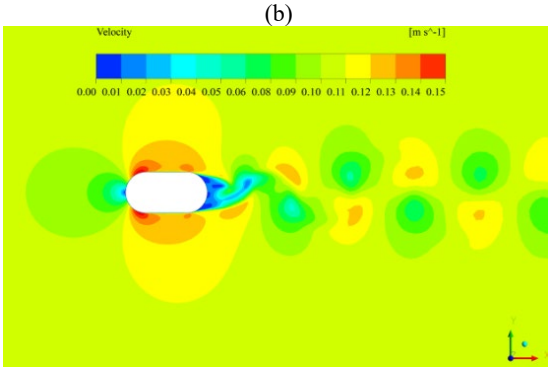

(c)

Fig.10 The visualized velocity contours of different shapes. (a) Shape based on the parametric method; (b) Ellipse; (c) Ear shape

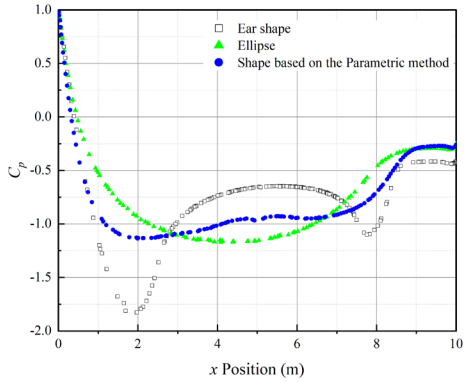

Fig.11 The mean pressure distribution along different SFT shapes

Fig.12 exhibits the skin friction coefficient (C_f) of different SFT cross-section shapes. C_f is defined by Eq.(6)

$$C_f = \frac{\tau_\omega}{\frac{1}{2}\rho U^2} \tag{6}$$

where τ_ω is the local wall shear stress.

The zero skin friction coefficient point indicates flow separation, vortices shedding downstream over the trailing edge and the subsequent vortex shedding region. It can be seen that the flow separation onset point of the ellipse occurs around x=8.4 m, followed by the ear shape at around x=8.6 m; while the parametric method shape occurs at around x=8.9 m, implying a noticeable forward flow separation region of the ellipse compared with the other shapes. Clearly, the SFT cross-section described by the parametric Bézier curve method has the most streamlined shape and the best flow attachment, which can further reduce the wake region size, and thus reduce the drag and lift.

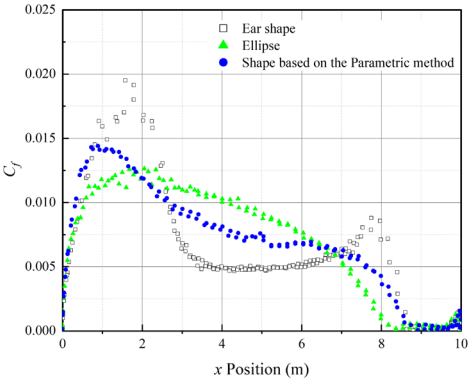

Fig.12 The skin friction distribution along different SFT shapes

It can be concluded that the SFT cross-section described by the parametric Bézier curve method has better hydraulic performances than the simpler shapes, and the ear shape is not recommended due to its uneven pressure distribution along the SFT cross-section surface and large $C_{l,rms}$ and $C_{d,m}$. However, more factors, such as material and construction cost, should also be considered in the cross-section optimization for practical engineering.

CONCLUSIONS

In this study, a parametric method based on the Bézier curve is firstly applied in the SFT cross-section geometry design, and then sensitivity analysis with various Bézier curve parameters is carried out. Finally, the hydraulic performance of SFT cross-sections defined by the

parametric Bézier curve and the simpler shapes including ellipse and ear shape are compared. The main conclusions are briefly summarized as follows:

(1) y_{up} equal to half of the total tunnel height results in a minimum $C_{l,rms}$ and $C_{d,m}$. For a fixed aspect ratio shape, a large b value should be avoided in the parametric SFT cross-section design.

(2) Good hydraulic performance of the SFT cross-section can't be achieved by continuously minimizing the leading edge radius, as flow bypassing the sharp apex and nadir will detach, and hence enlarge the wake region at the trailing edge.

(3) The SFT cross-section described by the parametric Bézier curve method has better hydraulic performance than the simpler shapes because of its streamlined shape and uniform pressure distribution along the SFT cross-section surface.

ACKNOWLEDGEMENTS

The study presented in this paper was conducted in the submerged floating tunnel research project led by China Communications Construction Company Ltd. (CCCC) and jointly carried out by universities, scientific research institutes, engineering consulting firms, design and construction companies in China and the Netherlands.

The authors would like to acknowledge C.J. Carlos Simão Ferreira for his contribution in elucidating the knowledge of airfoil design.

REFERENCES

American Association of State Highway Transportation Officials (2018), "A policy on geometric design of highways and streets".

Crighton, D. G. (1985). "The Kutta condition in unsteady flow". Annual Review of Fluid Mechanics, 17(1): 411-445.

Derksen, R. W., and Rogalsky, T. (2010). Bezier-PARSEC: An optimized aerofoil parameterization for design. Advances in engineering software, 41(7-8), 923-930.

Gang, L., Xiao-jun, Z., and Jian-xun, C. (2018). "The Dynamic Response of an Experimental Floating Tunnel with Different Cross Sections under Explosive Impact". Journal of Coastal Research, 82(sp1), 212-217.

James, W. D., Paris, S. W., and Malcolm, G. N. (1980). "Study of viscous crossflow effects on circular cylinders at high Reynolds numbers". AIAA Journal, 1980, 18(9): 1066-1072.

Jin, C., and Kim, M. (2018, July). Dynamic Responses of a Moored Submerged Floating Tunnel Under Moving Loads and Wave Excitations. In The 28th International Ocean and Polar Engineering Conference. International Society of Offshore and Polar Engineers.

Jin, C. K., Lee, J. Y., Kim, H. S., and Kim, M. H. (2017, July 31). Dynamic Responses of a Submerged Floating Tunnel in Survival Wave and Seismic Excitations. International Society of Offshore and Polar Engineers.

Jin, C., and Kim, M.-H. (2019, July 15). Tunnel-Mooring-Line-Vehicle Coupled Time-Domain Dynamic Analysis for a Submerged Floating Tunnel in Wave and Seismic Conditions. International Society of Offshore and Polar Engineers.

Jung, S., Choi, W., Martins-Filho, L. S., and Madeira, F. (2016). An Implementation of Self-Organizing Maps for Airfoil Design Exploration via Multi-Objective Optimization Technique. Journal of Aerospace Technology and Management, 8(2), 193-202.

Kang, S.-J., Kim, J.-T., An, J.-B., and Cho, G.-C. (2019, July 15). Numerical Study on Behavior of Ground Surrounding Interface Between Submerged Floating Tunnel and Subsea Bored Tunnel. International Society of Offshore and Polar Engineers.

Kharal, A., and Saleem, A. (2012). Neural networks based airfoil generation for a given Cp using Bezier–PARSEC parameterization. Aerospace science and Technology, 23(1), 330-344.

Li, K., and Jiang, X. (2016). Research on section form of submerged floating tunnels considering structural internal force optimization under fluid action. Procedia engineering, 166, 288-295.

Li, Q., Jiang, S., and Chen, X. (2018). Experiment on pressure characteristics of submerged floating tunnel with different section types under wave condition. Polish Maritime Research.

LUO, G., ZHOU, X., ZHANG, C., SHEN, Q. (2012). Numerical simulation analysis on rational cross-section of submerged floating tunnel. Railway Engineering, (12), 12. (in Chinese).

Ministry of Transport of the People's Republic of China (2010), "Guidelines for Design of Highway Tunnel". JTG/T D70—2010 (in Chinese).

Minoretti, A., Egeland, E. M., and Aasland, T. E. (2019, July). The Submerged Floating Tube Bridge for the Norwegian Fjords. In The 29th International Ocean and Polar Engineering Conference. International Society of Offshore and Polar Engineers.

Muhammad, N., Ullah, Z., and Choi, D. H. (2017). Performance evaluation of submerged floating tunnel subjected to hydrodynamic and seismic excitations. Applied Sciences, 7(11), 1122.

Nikolaev, N. V. (2019). Optimization of Airfoils along High-Aspect-Ratio Wing of Long-Endurance Aircraft in Trimmed Flight. Journal of Aerospace Engineering, 32(6), 04019090.

Pelletier, A., and Mueller, T. J. (2000). Low Reynolds number aerodynamics of low-aspect-ratio, thin/flat/cambered-plate wings. Journal of aircraft, 37(5), 825-832.

Tveit, P. (2000). Ideas on downward arched and other underwater concrete tunnels. Tunnelling and underground space technology, 15(1), 69-78.

Yan, H., Zhang, F., and Yu, J. (2016). The lectotype optimization study on submerged floating tunnel based Delphi method. Procedia engineering, 166, 118-126.